Navigation Using Deep-Space Optical Communication Systems

Sarah Elizabeth McCandless* and Tomas Martin-Mur†

Jet Propulsion Laboratory, California Institute of Technology, Pasadena, CA

This work investigates the deep-space spacecraft navigation performance achievable from tracking data types obtained using optical communication systems. These optical navigation types include ranging between spacecraft and a station on Earth and astrometric measurements of angular position. Two mission scenarios are analyzed: an interplanetary cruise trajectory for a Mars lander (Mars 2020), and a science orbit for a Mars orbiter (MAVEN). Various data types are simulated using comprehensive measurement models, tracking schedules, and geometrical constraints. Sensitivity analyses are performed to assess the effect of various contributors to measurement accuracy and navigation performance. For both of the mission scenarios studied, the optical navigation types yield equivalent or improved performance as compared to traditional radiometric observables, though radiometric data types slightly outperform optical observables during tracking data gaps in the science orbit scenario.

Deep-space optical communication data types have previously been proposed for deep-space navigation purposes, but those systems were not sufficient to replace radio frequency tracking systems. This analysis is a systematic, comprehensive investigation of the achievable performance for deep space missions. The analyses will enhance JPL's ability to assess the appropriateness of optically-based navigation for future missions and will be a critical piece of its navigation capabilities moving forward.

Nomenclature

a, b, c	Optical measurement uncertainty coefficients
D	Telescope diameter
DOR	Differential One-way Range
SRA	Sequential Ranging Assembly
T	Time
θ	Angle

I. Introduction

Ground-based radio-frequency tracking data has historically been the standard for deep-space navigation of spacecraft. Since the dawn of the space age in the 1960s, the National Aeronautics and Space Administration (NASA), as well as other institutions around the world, has used this data type, and this has enabled us to explore every planet in our solar system. NASA is now turning to laser communication, which allows higher volumes of scientific data transfer from deep space. The Optical Payload for Lasercomm Science (OPALS) was installed on the International Space Station (ISS) in April 2014 and successfully demonstrated laser communication systems between spacecraft in Low-Earth orbit (LEO) and ground stations,[1] and a first-generation optical communications terminal may be a component of the next Discovery mission, but as a technological demonstration.

*Navigation Engineer, Inner Planet Navigation, 4800 Oak Grove Dr., Pasadena, CA 91109

†Supervisor, Inner Planet Navigation, 4800 Oak Grove Dr., Pasadena, CA 91109

This study analyzes the accuracy of using optical ranging and ground-based astrometric measurements in place of traditional radiometric ranging, Doppler, and ΔDOR measurements for interplanetary navigation.

Previously, laser ranging using corner cube retro-reflectors has been used for precise orbit determination or Earth-orbiting spacecraft, achieving centimeter-level precision. Spacecraft astrometry has been used for assessment of orbital debris and for orbit determination of geostationary spacecraft,[2] while astrometry of natural bodies has been used for optical navigation in conjunction with on-board images. Additionally, some deep space laser ranging experiments were conducted with both the Mercury Laser Altimeter on MESSENGER[3],[4] with the Lunar Orbiter Laser Altimeter (LOLA) on the Lunar Reconnaissance Orbiter (LRO),[5] and the Lunar Laser Communications Demonstration on the Lunar Atmosphere Dust Environment Explorer (LADEE).[6] None of these systems, however, were designed to provide operational optical tracking capabilities sufficient to replace the radio-frequency tracking systems.

In contrast to these past uses, this work analyzes applications that are over much larger distances and using an active system instead of passive reflectors. For deep-space astrometry, future systems will not use the reflection of light from the Sun, but a laser signal transmitted by the spacecraft, allowing for a higher signal to noise ratio when filtering around the expected received laser frequency.

Two mission types are investigated here: Mars landing and Mars orbiter missions. These types are selected because the accuracy with which the mission trajectory needs to be reconstructed and predicted differs; Mars landing missions have much more demanding delivery requirements.

II. Radio Measurement Models

Traditional radiometric data types serve as the baseline measurements. Two-way Doppler, two-way SRA range, and ΔDOR are simulated for an interplanetary cruise trajectory for a Mars lander, while two-way Doppler and SRA range are simulated for a Mars orbiter in its science phase. The following measurement weights are assumed for baseline (Table 1) and no-margin (Table 2) cases for lander and orbiter (Table 3) missions. Elements highlighted in pink in Table 2 denote differences from baseline assumptions in Table 3. These measurements are simulated using the Mission Analysis, Operations, and Navigation Toolkit Environment (MONTE),[7] a multi-purpose software supporting the design and analysis of deep space missions. A key advantage of this study is using the same software for operational mission navigation and for the measurement simulation and covariance analysis. This enables analysis verification with actual mission data.[8]

III. Optical Measurement Models

Optical measurements are simulated using MONTE[7] as well. Deep space telecommunication system data types in this study include optical ranging and ground-based astrometric measurements of angular position. This is functionally equivalent to radio-ranging and ΔDOR observables. Optical range measurements are simulated using MONTE's 2-way range magnitude measurement, a high-precision 2-way light-time calculation that includes clock effects, ground and on-board delays, antenna offsets, and optional media corrections. A five minute integration time is used for the Mars lander cruise case and ten seconds for the Mars orbiter during the science orbit case.

Astrometric measurements are simulated using MONTE's Ra/Dec angle measurement, a high-precision 1-way light-time calculation that includes clock effects, ground delays, antenna offsets, and optional media corrections as well. Reference frame errors are also considered to take into account the alignment of the optical reference frame, that will be derived from the results of ESA's Gaia mission, to the VLBI frame that the planetary ephemeris are referred to. Astrometric measurement accuracy depends on elevation from the horizon, sky brightness, and angle between the Sun, spacecraft, and the Earth. Measurements are optimal within 30° of zenith, and ignored below 10° from the horizon. Additionally, measurements vary with sky brightness. They have deteriorated accuracy as the sky brightens, and are nearly impossible to record during the day. Sky brightness is characterized by the elevation of the Sun with respect to the horizon, and three periods are used in analysis: day, twilight, and night. Day is defined to be when the Sun is above the horizon, twilight is defined to be when the geometric center of the Sun is between 0° and 18° below the horizon, and night is defined to be when the Sun is at least 18° below the horizon. Finally, if the spacecraft is too close to the Sun, the angular measurements are difficult to obtain; for this reason, a 45° Sun keep-out constraint is used. Figure 1 is a schematic of these constraints. The figure shows that there may be whole

phases of interplanetary missions when astrometric observations may not be possible, if the angle between the Earth-to-spacecraft direction and the Earth-to-Sun direction is small. This could limit astrometric tracking for non-Type I Earth-Mars transfers missions, preclude astrometric tracking during final approach for Venus and Mercury missions, and impede astrometric tracking for outer planet missions for months at a time. The ground-based astrometry techniques analyzed in this research are also limited by the atmosphere, i.e. atmospheric refraction and turbulence. The elevation angle, θ_{el}, determines air mass, and as the mass increases, so do the differential chromatic error and turbulence. These limitations could be circumvented by using an optical terminal in Earth orbit, where it would not be affected by atmospheric effects and weather.

The uncertainty varies with sky brightness, and is defined for the categories described above. The uncertainty at night is defined in equation (1) below, where the parameters a_{night} and b_{night} are defined by equation (2). T is integration time and D is telescope size. These equations ignore the effect of moon light.

$$\epsilon^2_{\text{night}} = a_{\text{night}} + \frac{b_{\text{night}}}{\sin^2\theta_{el}} \tag{1}$$

$$a_{\text{night}} \sim 0.75\left(\frac{1\text{ m}}{D}\right)^2\left(\frac{1\text{ hour}}{T}\right)\text{mas}^2, b_{\text{night}} \sim 0.25\left(\frac{1\text{ m}}{D}\right)^2\left(\frac{1\text{ hour}}{T}\right)\text{mas}^2 \tag{2}$$

During the day, the brightness of a clear sky (ignoring clouds) depends on the Sun angle, θ_{Sun}, the angle between the line of sight of the spacecraft and the vector pointing to the Sun. This angle must be larger than 45°, per the keep-out constraint previously mentioned. Additionally, the instrument only operates with a minimum θ_{Sun} angle of 20°. Errors in this regime are mainly due to noise from the sky background and air turbulence. For a 5 m telescope, the uncertainty is defined by equation (3), where the parameters are defined in equation (4).

$$\epsilon^2_{\text{day}} = a_{\text{day}} + \frac{b_{\text{day}}}{\sin^2\theta_{el}} + c_{\text{day}}\cos^2\theta_{el} \tag{3}$$

$$a_{\text{day}} \sim 6.6\left(\frac{1\text{ hour}}{T}\right)\text{mas}^2, b_{\text{day}} \sim \left(\frac{1\text{ hour}}{T}\right)\text{mas}^2, and c_{\text{day}} \sim 3.6\left(\frac{1\text{ hour}}{T}\right)\text{mas}^2 \tag{4}$$

During twilight, a linear interpolation between day and night is performed based on the Sun-below-horizon angle, θ_{sbh}.

$$\epsilon^2_{\text{twilight}} = \epsilon^2_{\text{day}}\left(1 - \frac{\theta_{sbh}}{18^\circ}\right) + \epsilon^2_{\text{night}}\frac{\theta_{sbh}}{18^\circ} \tag{5}$$

These equations were provided by Chengzing Zhai.[9] In this analysis, the nominal value for telescope diameter is set to 5.0 m and the nominal value for integration time is set to 360 seconds. Immediately prior to publication, it was noted that the integration time should reflect the value used in the measurement simulation (i.e. 5 minutes for the interplanetary cruise trajectory and 10 seconds for the science orbit). It is more significant for the science orbit, but does not have a significant impact.

Error sources are similar to those for radiometric measurements. The troposphere affects astrometric measurement noise and biases, and is accounted for in the measurement weights. It does not need to be explicitly corrected since the spacecraft position is measured against the star background. Ionospheric and solar plasma effects are negligible at optical frequencies, though they are more pronounced for radiometric data. Global and regional error levels in the star catalog are considered as well. Finally, station position, clock, Earth orientation parameter, planetary ephemeris, and spacecraft dynamic errors are considered just as for radiometric measurements. Error assumptions for optical parameters are shown in Table 4.

The analyses described in this study do not take into account the effect of weather on the availability of optical data. It is assumed that at all times a ground station with clear sky will be available to perform the measurements. This could be accomplished by having multiple telescopes within the footprint of the returned laser signal, by performing dynamic scheduling of the tracking passes that takes into account local weather, and also by optimal siting of the optical terminals. While radio-frequency telescopes and tracking stations are sited in valleys in order to reduce interference from other radio emitters, optical telescopes and terminals benefit from being sited at dry mountain tops so they can be most of the time above the cloud level and the effects of atmospheric dispersion and attenuation can be reduced.

IV. Mars Lander Case Study

The more rigorous analysis case is for a Mars lander. This analysis is based on NASA's next Mars rover, Mars 2020. It is scheduled to launch in late summer 2020 and arrive in early spring 2021. Initially we were planning to use an Earth-Mars transfer for the 2022 opportunity, but the optimal transfer for that opportunity resulted in a Type-II trajectory for which the Mars encounter happens at a spacecraft-Earth-Sun angle that precludes astrometric measurements. The measurement simulation schedule follows what is expected in operations. Continuous coverage is provided immediately following launch, around Trajectory Correction Maneuvers (TCMs), and for the final 45 days. The majority of cruise is covered with daily coverage. Daily passes are possible Mondays, Tuesdays, Wednesdays, Fridays, and Saturdays and pass lengths are four hours. The full schedule is shown in Table 5. This schedule is followed when simulating both radio and optical data.

A sensitivity analysis is performed to assess the impact of data types and weights. The baseline case is radiometric data (Two-way Doppler, SRA range, and ΔDOR) only. An optical only (optical range and astrometric measurements), astrometry only, optical range only, and SRA range and ΔDOR cases are analyzed as well. Each data combination is evaluated with baseline and no-margin parameters. Variations on telescope diameter (and subsequently angular uncertainties) and optical range weight are also implemented. Larger telescope diameters reduce uncertainties, but they are more expensive to construct and maintain. A summary of evaluated cases is presented in Table 6.

To achieve a landing at a targeted site, orbit determination analyses target a specific entry time and B-plane aimpoint that correspond to an entry flight path angle (EFPA) and latitude and longitude on the surface. These atmospheric entry interface conditions are derived from the desired landing site and an iteration of an open-loop simulation of the entry, descent, and landing (EDL) trajectory that produces the required EFPA and matches the state vector of the interplanetary trajectory at entry. The B-plane, or Body Plane, is a plane normal to the incoming asymptote of the hyperbolic orbit and contains the target body's center of mass. Atmospheric entry state knowledge accuracy is the orbit determination knowledge accuracy (measured by the position or velocity covariance norm) at entry based on an OD data cutoff of Entry - 6 hours. The knowledge accuracy at TCM5 includes the effects of the final maneuver (executed at Entry - 2 days). For Mars 2020 and MSL, the EFPA has an uncertainty requirement of ± 0.20 deg (3σ).

Figures 2, 3, and 4 show the 3σ B-plane error ellipses, i.e. the delivery accuracy ellipses, for the TCM5 knowledge case. It is immediately apparent from Figure 4 that the astrometry-only case is poor in the $B \cdot T$ direction, while the other combinations are poorer in the $B \cdot R$ direction. The Earth is in the $B \cdot T$ direction, and the angular measurements are plane-of-sky measurements, resulting in poor localization (i.e. from Earth, there is good angular resolution, but poor depth of field). A ΔDOR only case is not considered, but would show similar behavior. Comparing the optical only case to the radio only case, we see that the optical case is improved in both directions. The improvement in the $B \cdot R$ direction implies that the astrometric measurements are potentially better than their ΔDOR radiometric equivalents.

As Figure 3 shows, different parameters have varying affects on the optical performance. The largest contributor is telescope size; a degraded telescope diameter of 1.0 m results in performance similar to that achieved using radiometric observables (it is improved in the $B \cdot R$ direction and degraded in the $B \cdot T$ direction). Conversely, an improved telescope diameter of 10.0 m has improved performance over the no-margin case. Frame effects have negligible impacts at the level that they are considered, and optical range weights have little impact.

V. Mars Orbiter Case Study

This analysis is based on the Mars Atmosphere and Volatile Evolution (MAVEN) mission, currently in orbit at Mars. It launched in November 2013 and has been operating at Mars since September 2014. MAVEN has a 4.6 hr period, an equatorial inclination of 75°, an eccentricity of 0.47, and a periapsis altitude of about 160 km. This orbit is designed to give an atmospheric density at periapsis between 0.05 and 0.15 kg/km^3.

The measurement simulation schedule follows the operations schedule by scheduling daily passes. Operational passes are eight hours long, but the optical data simulation rarely is able to maintain a pass of that duration. A much shorter pass is required–two hours. This poses potential operational constraints, which will be discussed in the following section. While the radio simulation does not have this constraint (passes of longer durations are possible), a two hour pass is simulated in this study for consistency between the data

types. A smaller subset of data types are simulated for the orbiter study; astrometric data is not simulated because it is not necessary (the radiometric analog, ΔDOR is not used in operations). Both two-way Doppler and SRA range are simulated. Measurement model assumptions are the same, except where noted in Table 3, and the measurement integration time is shortened to 10 seconds.

State covariance norms are calculated for reconstructed and predicted orbits. MAVEN is required to reconstruct trajectories to within 3 km, but the prediction requirements are more involved and in terms of orbital elements: predict semi-major axis to within 50 km, eccentricity to within 0.025, inclination to within 0.20°, longitude of ascending node to within 0.04°, and argument of periapsis to within 0.3°. The first reconstruction case is from April 18, 2016 08:00 to April 19, 2016 15:00. The state (position and velocity) norms and position component norms (radial, transverse, and normal), as well as the data passes (roughly two hours in duration), are shown in Figure 5 and Figure 6. The optical data outperforms its radio counterpart–even during data gaps–and Table 7 shows the improvement. May 4 - 6, 2015 corresponds to orbits 1154 - 1162, and April 18 - 19, 2016 corresponds to orbits 3018 - 3024.

Another reconstruction case was analyzed from May 5, 2015 to May 6, 2015 12:00. This was a period of degraded OD performance due to occultations. As seen in Figure 7 and Figure 8, optical does outperform radio during tracking data passes, but not during tracking gaps. This may be a result of the poor geometry, or it may be the result of an extended tracking data gap (see Table 8). May 4 - 6, 2015 corresponds to orbits 1154 - 1162, and April 18 - 19, 2016 to orbits 3018 - 3024. Even with this degraded performance, the optical data easily meets the reconstruction requirement of 3 km.

A prediction case was created by running out the April 2016 reconstruction case an additional two and a half days to April 22, 2016 6:00 (MAVEN has a 20 second periapsis timing requirement that can nominally be met within 2.5 days). Figure 9 shows these elements. The optical data outperforms the radio measurements (in some instances, by orders of magnitude). Sensitivity analyses are slightly simplified for the orbiter case as only optical range is used. For both reconstruction and prediction cases, modifying the optical range weight had little impact, which is consistent with the performance for the Mars 2020 cruise trajectory.

A. Orbiter Operational Constraints

There are some additional operational constraints that must be considered for an orbiter. MAVEN, like other Mars-orbiting missions, requires a long duration pass to ensure they are not sensitive to DSN related problems (connectivity issues, station outages, missed passes etc.) A two-hour long pass is not long enough to provide satisfactory robustness. Additionally, this analysis assumes all passes are able to be used for navigation when that may not be the case. As an example, MAVEN currently averages 9 DSN passes per week (once daily with two additional passes for margin), but only two of those are earth-pointed high-gain antenna (HGA) passes, while the others are performed using a low-gain antenna. MAVEN does not have a gimbaled HGA, so HGA communications with Earth require rotating the entire spacecraft, preventing desired science measurements. An optical communication system would also require either a gimbal, adding complexity, or the rotation of the whole spacecraft in order to support tracking, precluding science observations during that time.

VI. Conclusion

Optical tracking data types could be viable alternatives to radiometric data types for interplanetary navigation. If they are available, optical range and astrometric measurements can be utilized as frequently as their radiometric counterparts for interplanetary trajectory analysis. Optical range may be a valuable data type for orbiting missions, but there are additional operational constraints to consider. Sensitivity analyses show optical measurements to be an improvement over radiometric measurements for both Mars landers and Mars orbiters, though for Mars orbiters in particular, pass frequency and pass duration have a large influence. Depending on gap duration and planetary geometry, optical data types show improved performance over radiometric data during tracking data gaps, as well.

Acknowledgements

The navigation work described in this paper was carried out at the Jet Propulsion Laboratory, California Institute of Technology, under a contract with the National Aeronautics and Space Administration.

Copyright 2016. California Institute of Technology.

References

[1]Abrahamson, M. J., Oaida, B. V., Sindiy, O., and Biswas, A., "Achieving operational two-way laser acquisition for OPALS payload on the International Space Station," *Proc. SPIE*, Vol. 9354, 2015, pp. 935408–935408–21.

[2]Alby, F. et al., "Status of CNES optical observations of space debris in geostationary orbit," *Adv. Space Res.*, Vol. 34, 2004, pp. 1143–1149.

[3]Smith, D. et al., "Two-Way Laser Link over Interplanetary Distance," *Science*, Vol. 311, 2006, pp. 311.

[4]Cavanaugh, J. et al., "The Mercury Laser Altimeter instrument for the MESSENGER mission," *Space Sci. Rev.*, Vol. 131, 2007, pp. 451–480.

[5]Zuber, M. et al., "The Lunar Reconnaissance Orbiter Laser Ranging Investigation," *Space Sci. Rev.*, Vol. 150, 2010, pp. 63–80.

[6]Boroson, D. M., Robinson, B. S., Murphy, D. V., Burianek, D. A., Khatri, F., Kovalik, J. M., Sodnik, Z., and Cornwell, D. M., "Overview and results of the Lunar Laser Communication Demonstration," *Proc. SPIE*, Vol. 8971, 2014, pp. 89710S–89710S–11.

[7]Evans, S. et al., "MONTE: The Next Generation of Mission Design & Navigation Software," *The 6th International Conference on Astrodynamics Tools and Techniques (ICATT)*, 2016.

[8]Martin-Mur, T. et al., "Mars Science Laboratory Interplanetary Navigation," *Journal of Spacecraft and Rockets*, Vol. 51L4, 2014, pp. 1014–1028.

[9]Zhai, C., "Uncertainties of ground-based astrometry," Tech. rep., Jet Propulsion Laboratory, 2016.

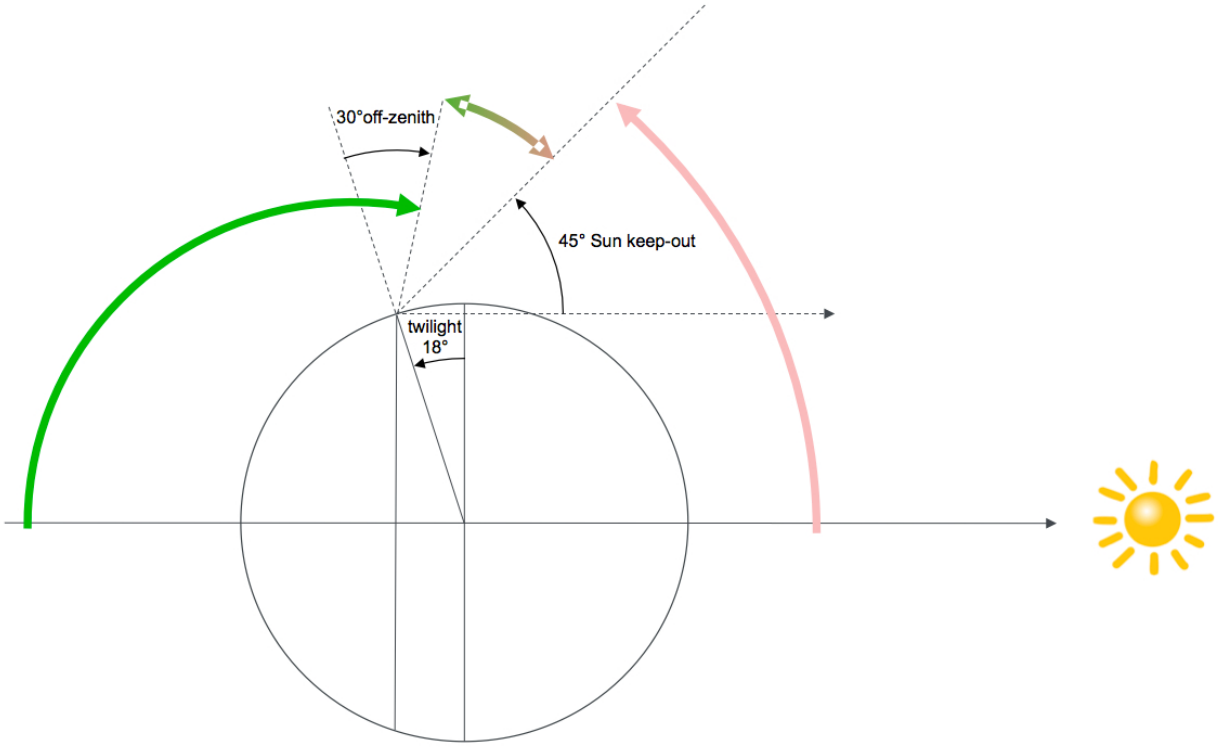

Figure 1. Geometric Constraints

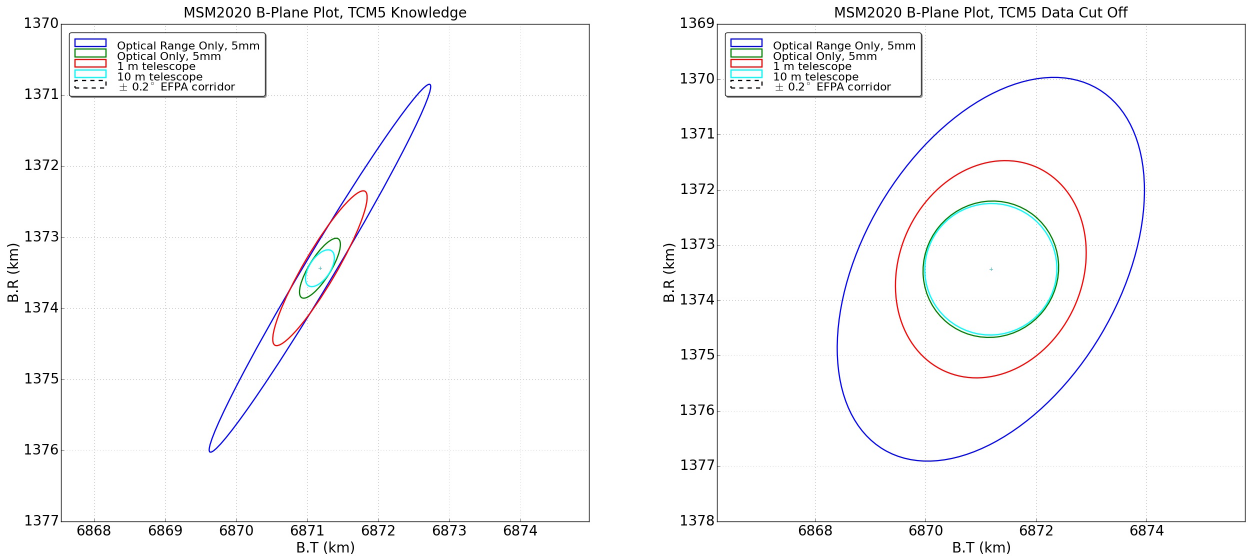

Figure 2. B-Plane Plots for Sensitivity Analysis. Nominal optical range weight is 5.0 cm. As expected, the improved range weight improves OD performance. These plots show the results for both the TCM-5 Knowledge and TCM-5 Delivery cases.

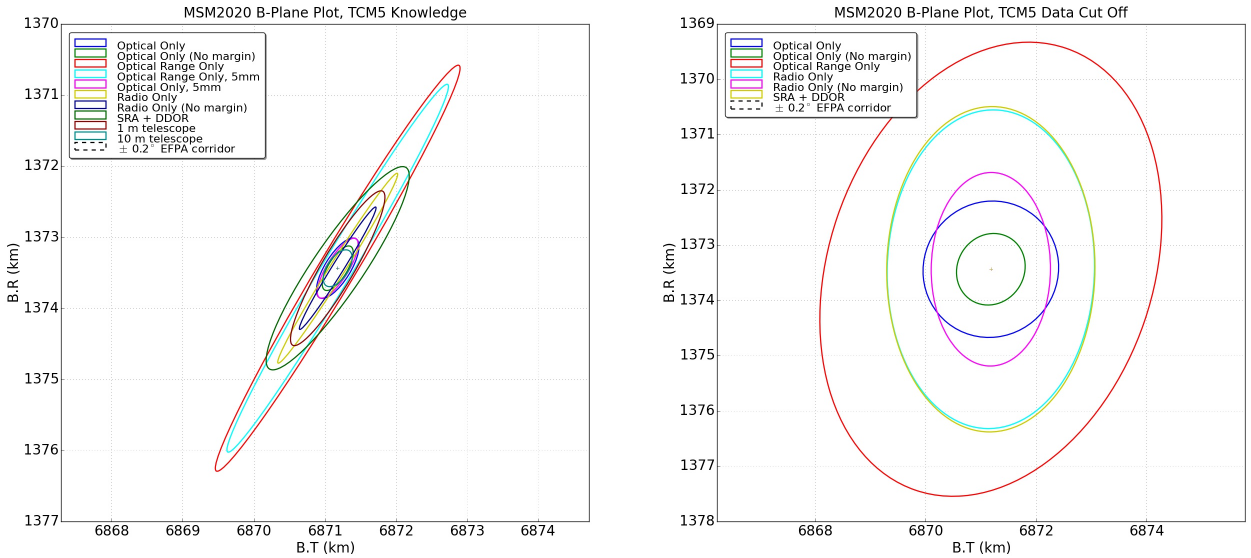

Figure 3. B-Plane Plots for Data Combination Analysis. Various combinations of radiometric and optical observables are compared. These plots show the results for both the TCM-5 Knowledge and TCM-5 Delivery cases.

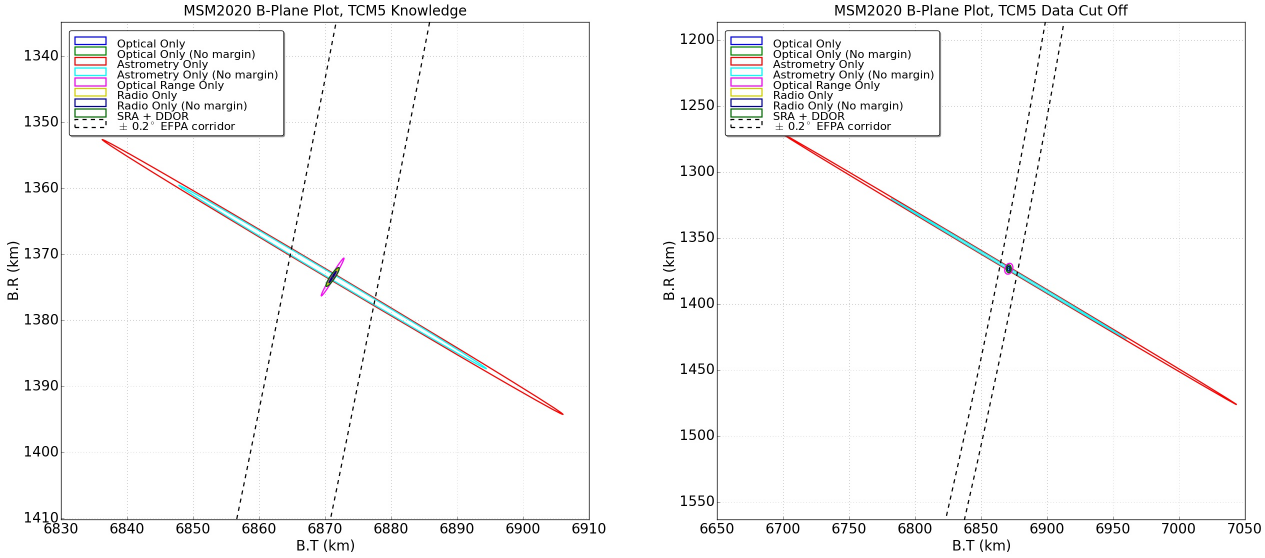

Figure 4. B-Plane Plots for Data Combination Analysis, including an astrometric only case. These plots show the results for both the TCM-5 Knowledge and TCM-5 Delivery cases.

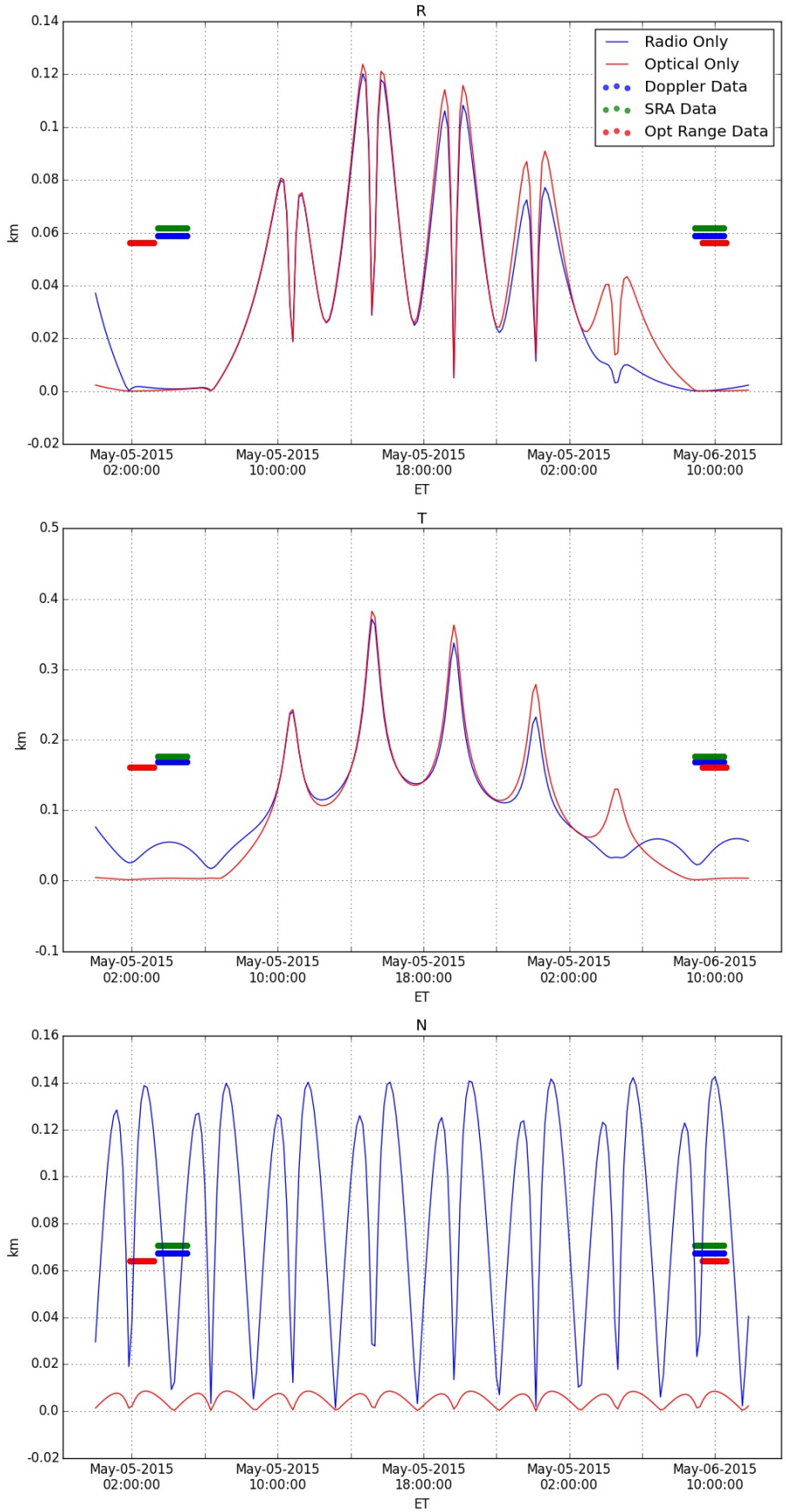

Figure 5. April 18 – 19, 2016 Reconstruction Position Covariance Norms in RTN Frame

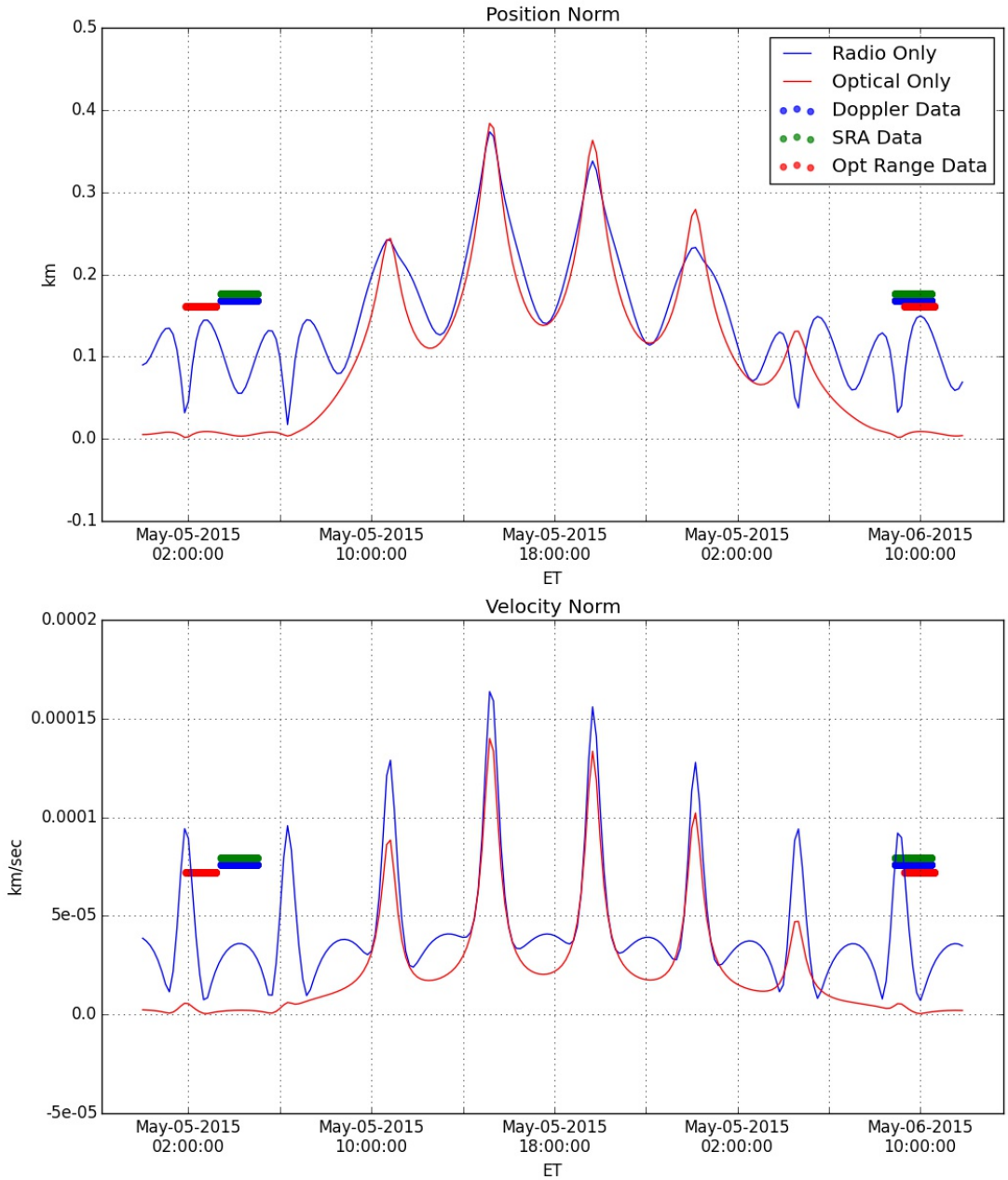

Figure 6. April 18 – 19, 2016 Reconstruction Position and Velocity Covariance Norms

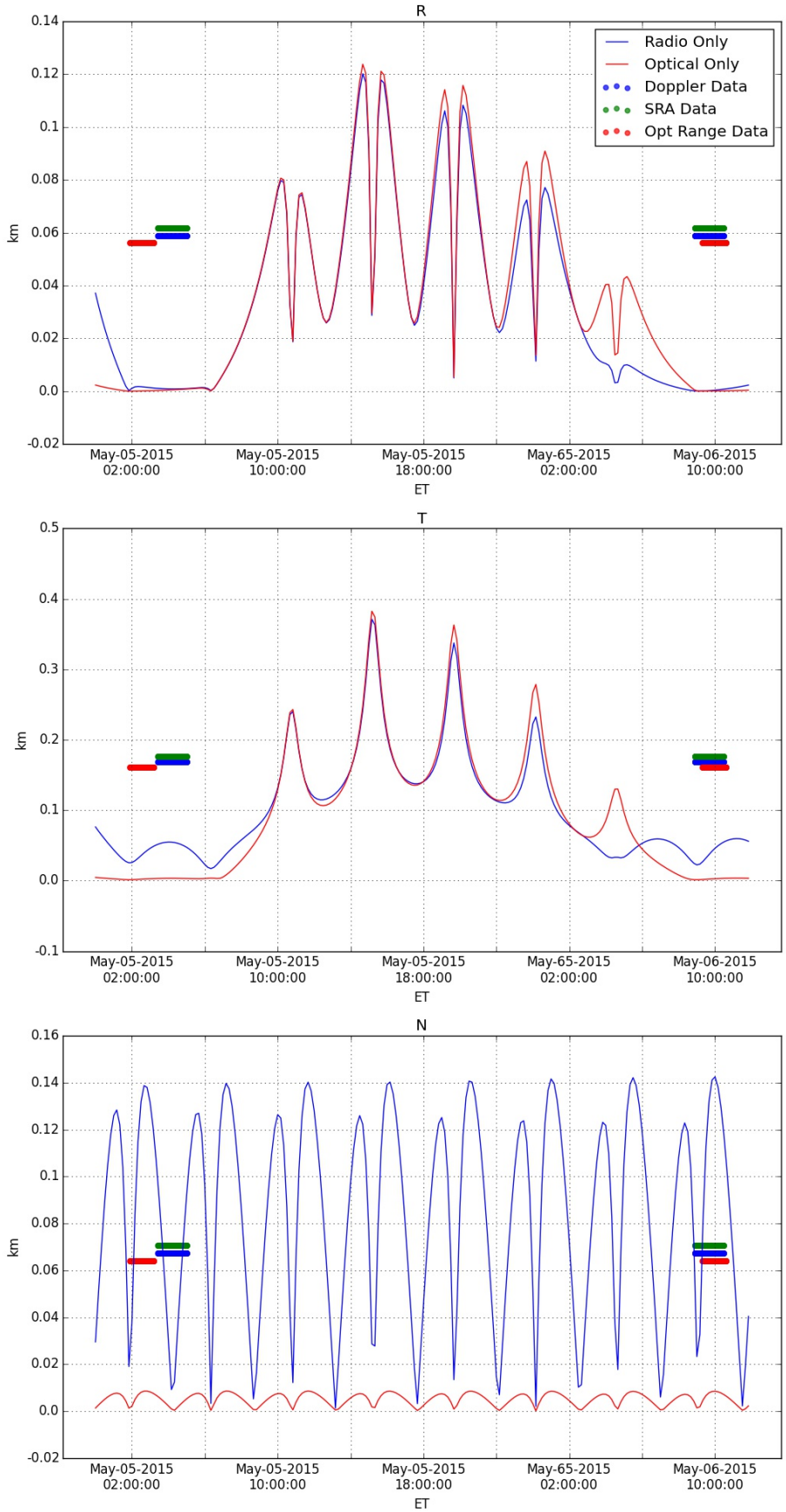

Figure 7. May 5 – 6, 2015 Reconstruction Position Covariance Norms in RTN Frame

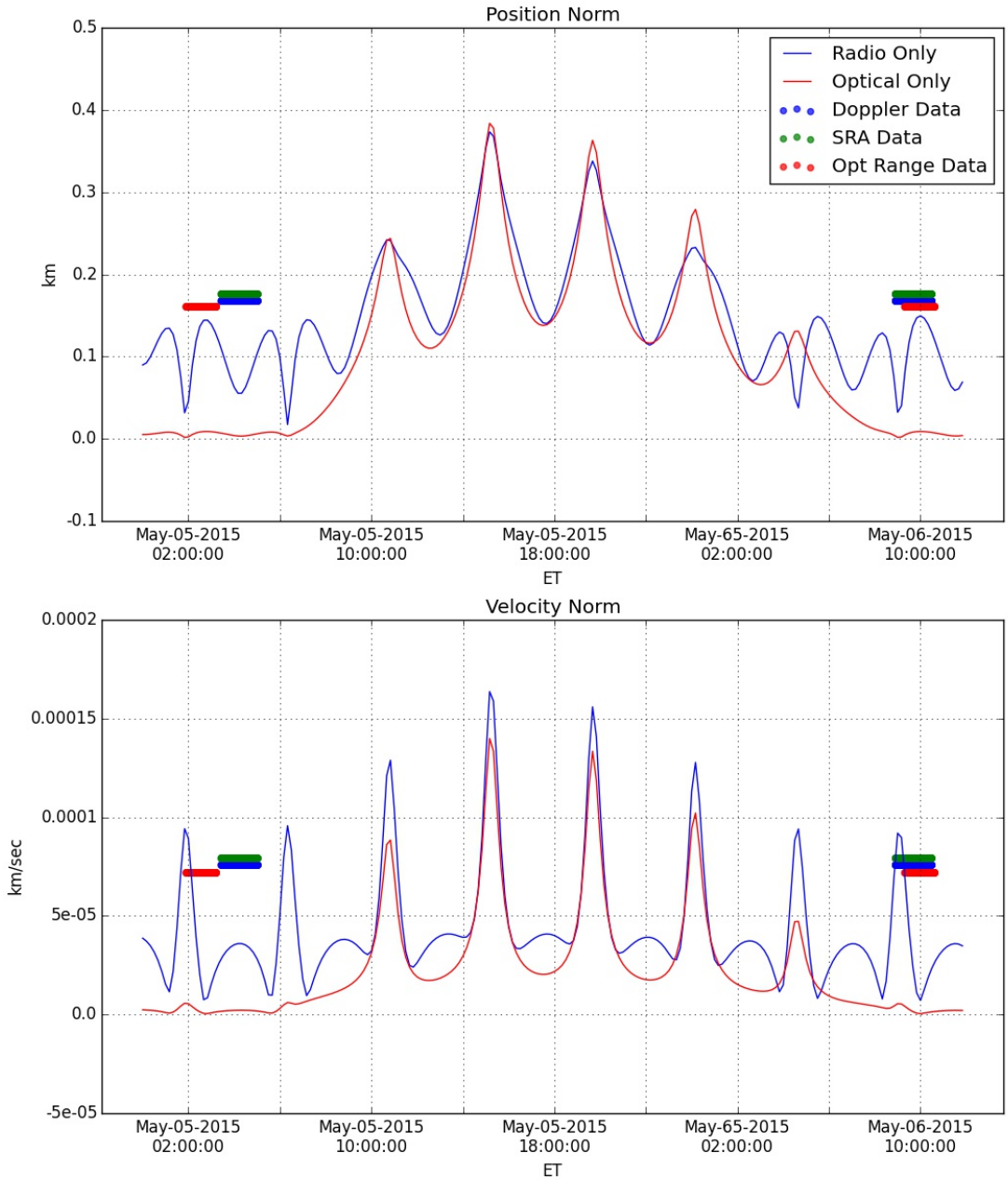

Figure 8. May 5 – 6, 2015 Reconstruction Position and Velocity Covariance Norms

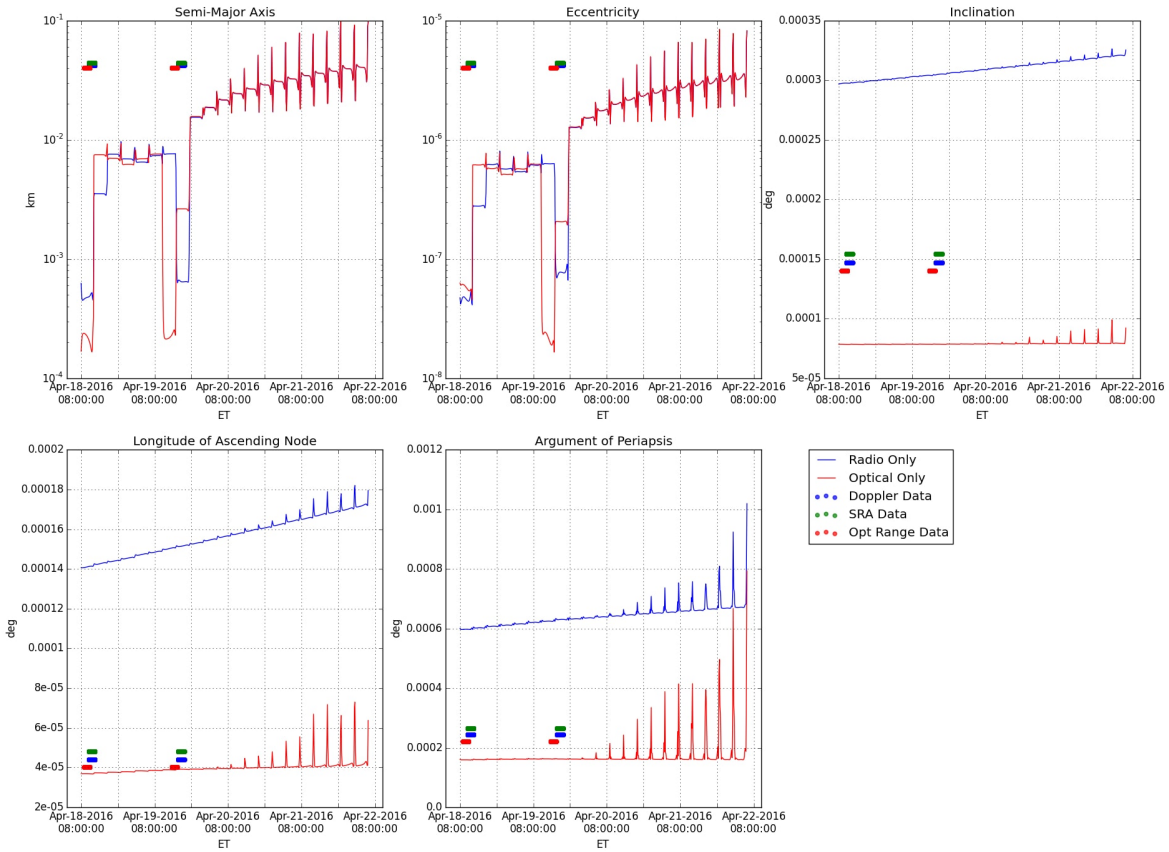

Figure 9. April 18 – 22, 2016 Prediction Accuracy

Table 1. Baseline Orbit Determination Error Assumptions

Error Source	Estimate or Consider	A Priori Uncertainty (1σ)	Correlation Time	Update Time	Comments
Epoch state position	Est.	1000 km	-	-	
Epoch state velocity	Est.	1 km/s	-	-	
X-Band 2-way Doppler	-	0.1 mm/s	-	-	0.0056 Hz
Range	-	3 m	-	-	21.03 RU, low SNR during late cruise
ΔDOR	-	60 ps	-	-	$\sim$2.4 nrad
Doppler Bias	Est.	0.002 mm/s	0	Per pass	Residual error from spin bias estimation
Range Bias	Est.	2 m	0	Per pass	DSN performance
Station Locations	Con.	Full 2003 cov.	-	-	
Quasar Locations	Con.	1 nrad	-	-	
Pole X, Y	Est.	1-4 cm	48 hr	6 hr	Slope 2 days before EOP to EOP + 12 hr
UT1	Est.	1.7-15 cm	48 hr	6 hr	Slope 6 days before EOP to EOP + 12 hr
Ionosphere day/night	Est.	55/15 cm	6 hr	1 hr	S-band units; use 6x (iono) and 2x (trop) apsig when no actuals; subsequent passes uncorrelated
Troposphere wet/dry	Est.	1/1 cm	6 hr	1 hr	
Mars and Earth Ephemerides	Con.	DE423 Covariance	-	-	
Mars GM	Con.	2.80×10^{-4} km^3/s^2	-	-	$\sim$10x MGS95J formal error
Solar Pressure					High-fidelity model
Radial (Gr)	Est.	5%	7 days	1 day	Correlation broken at turns. Gr and Gx estimated as both a bias and a stochastic
Tangential (Gx)	Est.	5%	7 days	1 day	
Out of plane (Gy)	Est.	1%	-	-	
Non-gravitational Accelerations	-	0 km/s^2	-	-	Accommodated in SRP model
ACS Event ΔV	Every 7 days from L+15 days until E-2 days				Conservative assumption
Per axis	Est.	2 mm/s before E-45 days 1 mm/s after E-45 days	-	-	Flight system requirement
Maneuver execution errors					Range of values for current set of cases
TCM-4 (E-8d)	Est.	2.32-2.43 mm/s	-	-	5% proportional error and 4 mm/s fixed error (3σ), vector mode maneuver
TCM-5 (E-2d)	Est.	1.910-1.912 mm/s	-	-	

Table 2. No-Margin Orbit Determination Error Assumptions

Error Source	Estimate or Consider	A Priori Uncertainty (1σ)	Correlation Time	Update Time	Comments
Epoch state position	Est.	1000 km	-	-	
Epoch state velocity	Est.	1 km/s	-	-	
X-Band 2-way Doppler	-	0.05 mm/s	-	-	2.81 mHz, MER performance
Range	-	3 m	-	-	21.03 RU, low SNR during late cruise
ΔDOR	-	40 ps	-	-	~1.6 nrad, Expected performance on 70m and BWG with improved LNAs and newly-engineered microwave feed systems
Doppler Bias	Est.	-	-		Not needed when the spin rate estimation error is negligibly small
Range Bias	Est.	1 m	0	Per pass	Expected DSN performance
Station Locations	Con.	Full 2003 cov.	-	-	
Quasar Locations	Con.	1 nrad	-	-	
Pole X, Y	Est.	1 cm	48 hr	6 hr	No change from fit to predict
UT1	Est.	1.7-7.5 cm	48 hr	6 hr	Slope 6 days before EOP to EOP + 12 hr
Ionosphere day/night	Est.	55/15 cm	6 hr	1 hr	S-band units; use 6x (iono) and 2x (trop) apsig when no actuals; subsequent passes uncorrelated
Troposphere wet/dry	Est.	1/1 cm	6 hr	1 hr	
Mars and Earth Ephemerides	Con.	0.5 x DE414 Covariance	-	-	Assumes improvement with additional 1/month ΔDOR to MRO and Odyssey
Mars GM	Con.	2.80×10^{-4} km^3/s^2	-	-	~10x MGS95J formal error
Solar Pressure					High-fidelity model
Radial (Gr)	Est.	2%	7 days	1 day	Correlation broken at turns. Gr and Gx estimated as both a bias and a stochastic
Tangential (Gx)	Est.	2%	7 days	1 day	
Out of plane (Gy)	Est.	1%	-	-	
Non-gravitational Accelerations	-	0 km/s^2	-	-	Accommodated in SRP model
ACS Event ΔV	First turn at L+15 days, then every 7 days until E-8 days				Conservative assumption
Per axis	Est.	0.1 mm/s before E-45 days	-	-	MER-B worst case performance
Maneuver execution errors					Range of values for current set of cases
TCM-4 (E-8d)	Est.	1.68-2.32 mm/s	-	-	5% proportional error and 2
TCM-5 (E-2d)	Est.	0.99-1.03 mm/s	-	-	mm/s fixed error (3σ), vector mode maneuver

Table 3. Orbiter Baseline Orbit Determination Error Assumptions

Error Source	Estimate or Consider	A Priori Uncertainty (1σ)	Correlation Time	Update Time	Comments
Epoch state position	Est.	100 km	-	-	
Epoch state velocity	Est.	0.1 km/s	-	-	
X-Band 2-way Doppler	-	0.2 mm/s (60 sec)	-	-	0.0056 Hz
Station Locations	Con.	Full 2003 cov.	-	-	
Earth Orientation	Con.	10cm	-	-	X/Y-pole, UT1
Ionosphere day/night	Con.	65/15 cm	-	-	
Troposphere wet/dry	Est.	4/1 cm	-	-	
Mars and Earth Ephemerides	Con.	DE414 Covariance	-	-	
Mars GM	Con.	10×10 covariance	-	-	$\sim$20x MGS95J formal error, Include GM
Orbit Trim Maneuvers	-	-	-	-	Not Included
Solar Radiation Overall	Est.	10%	White	18 hours	
Scale Factor (%)	Stochastic	10%			
Density	Est.	13.3%	White	Per Orbit	Est. for reconstruct only
Scale Factor (%)	Stochastic	35%			
Small Forces (DESAT)	Stochastic	0.67 mm/s	White	Per Orbit	

Table 4. Optical Baseline Orbit Determination Error Assumptions

Error Source	Estimate or Consider	A Priori Uncertainty (1σ)	Correlation Time	Update Time	Comments
Range	-	5.0 cm	-	-	
Celestial Frame	Con.	0.1×10^{-9} rad	-	-	

Table 5. Interplanetary Trajectory Measurement Simulation Schedule

Dates	Pass Type
7/19/20 – 8/16/20	Continuous
8/16/20 – 9/13/20	Daily
9/13/20 – 9/17/20	Continuous
9/17/20 – 12/18/20	Daily
12/18/20 – 12/22/20	Continuous
12/22/20 – 1/4/21	Daily
1/4/21 – 2/18/21	Continuous

Table 6. Sensitivity Cases, including data combinations and sigma changes

Case	Modification
Data Combination	Radio Only
Data Combination	Optical Only
Data Combination	Astrometry Only
Data Combination	Optical Range Only
Data Combination	SRA Range + ΔDOR
Optical Only	5mm range weight
Optical Only	1m telescope
Optical Range Only	5mm range weight

Table 7. State covariance norm comparison between optical and radio data types. Positive values indicate optical has improved performance.

Parameter	3018 – 3024	1154 – 1162
Position Norm	20%	15%
Velocity Norm	15%	31%
Radial Position	4%	-8%
Tangential Position	21%	-4%
Normal Position	29%	94%

Table 8. Reconstruction Data Gap Durations.

Data Type	3018 – 3024	1154 – 1162
Doppler	23:04:30	27:52:40
Range	23:04:27	27:52:45
Optical Range	25:14:30	30:06:00